Available online at www.sciencedirect.com

ScienceDirect

Proceedings of the Combustion Institute 39 (2023) 2991–2999

Proceedings of the Combustion Institute

www.elsevier.com/locate/proci

Effects of cryogenic temperature on premixed hydrogen/air flame propagation in a closed channel

Linlin Yang, Zheng Chen*

SKLTCS, CAPT, College of Engineering, Peking University, Beijing 100871, China

Received 6 January 2022; accepted 31 August 2022
Available online 26 October 2022

Abstract

As a carbon-free fuel, hydrogen has received significant attention recently since it can help enable low-carbon-economy. Hydrogen has very broad flammability range and very low minimum ignition energy, and thereby there are severe safety concerns for hydrogen transportation and utilization. Cryo-compressed hydrogen is popularly used in practice. Therefore, it is necessary to investigate the combustion properties of hydrogen at extremely low or cryogenic temperatures. This study aims to assess and interpret the effects of cryogenic temperature on premixed hydrogen/air flame propagation and acceleration in a thin closed channel. Different initial temperatures ranging from normal temperature ($T_0 = 300$ K) to cryogenic temperature ($T_0 = 100$ K) are considered. Both one- and two-dimensional hydrogen/air flames are investigated through transient simulations considering detailed chemistry and transport. It is found that when the initial temperature decreases from $T_0 = 300$ K to $T_0 = 100$ K, the expansion ratio and equilibrium pressure both increase substantially while the laminar flame speeds relative to unburned and burned gasses decrease moderately. The one-dimensional flame propagation is determined by laminar flame speed and thereby the combustion duration increases as the initial temperature decreases. However, the opposite trend is found to happen to two-dimensional flame propagation, which is mainly controlled by the flame surface area increase due to the no-slip side wall constraint and flame instability. Based on the change in flame surface area, three stages including the initial acceleration, steady burning and rapid acceleration are identified and investigated. It is demonstrated that the large expansion ratio and high pressure rise at cryogenic temperatures can significantly increase the flame surface area in early stage and promote both Darrieus-Landau instability (hydrodynamic instability) and Rayleigh-Taylor instability in later stage. These two instabilities can substantially increase the flame surface area and thereby accelerate flame propagation in hydrogen/air mixtures at cryogenic temperatures. The present study provides useful insights into the fundamental physics of hydrogen flames at extremely low temperatures, and is closely related to hydrogen safety.

Keywords: Hydrogen safety; Cryogenic temperature; Premixed flame; Flame-pressure waves interaction; Flame instability

---

1. Introduction

Recently, hydrogen has drawn significant attention since there is no carbon emission in its utilization [1]. Compared to hydrocarbon fuels, hy-

---

* Corresponding author.
E-mail address: cz@pku.edu.cn (Z. Chen).

https://doi.org/10.1016/j.proci.2022.08.091

drogen has much lower ignition energy, broader flammability range and higher reactivity [2]. Therefore, there are severe safety concerns for hydrogen utilization [3,4]. To ensure safe utilization of hydrogen and mitigate potential hydrogen fire hazards, it is of paramount importance to understand the combustion properties of hydrogen relevant to its storage and transportation [5]. For instance, hydrogen is highly diffusive and the leaked hydrogen can be easily ignited in ambient air due to its very low minimum ignition energy. Besides, cryo-compressed hydrogen is popularly used for storage and transportation of large amount of hydrogen. Therefore, it is necessary to investigate the combustion properties of hydrogen at extremely low temperatures. This motivates the present study on premixed hydrogen/air flame propagation at normal and cryogenic temperatures.

In the literature, there are many studies on cryogenic hydrogen [3,4]. For examples, Friedrich et al. [6] experimentally studied the release and ignition of cryogenic hydrogen jets at temperatures of 35∼65 K. They identified three combustion regimes which appear after ignition of cryogenic hydrogen jets. Panda and Hecht [7] investigated the ignition and flame characteristics of under-expanded cryogenic hydrogen jets and found that the jet flames of very cold hydrogen are completely different from those of atmospheric temperature hydrogen. Ren and Wen [8] conducted high-resolution simulations to investigate the transient flow structures of under-expanded cryogenic hydrogen jets. Besides, self-ignition might happen during the sudden release of high-pressure hydrogen [9]. The self-ignition is mainly caused by shock waves and the interaction among them; and it has been extensively studied for pressurized hydrogen at normal temperature (e.g., [10]).

The above studies mainly focused on ignition and flame while there is little work on detonation in cryogenic hydrogen. Detonation has very high overpressure and thereby is extremely destructive. Therefore, preventing and mitigating detonation in hydrogen is of crucial importance for safe hydrogen utilization. Though extensive efforts have been devoted to fast flame propagation and deflagration-to-detonation transition (DDT) in H_2/air mixtures at normal temperatures (see [5,11] and references therein), much less attention was paid to DDT and detonation properties of hydrogen at extremely low temperatures. Recently, Kuznetsov et al. [12,29] have studied the flame acceleration and detonation development in H_2/air mixtures at cryogenic temperatures from 80 to 130 K in a shock tube. Besides the cryogenic temperatures, they also conducted experiments at ambient temperature in order to provide the reference data for cryogenic experiments. Interestingly, they found that the run-up-distance to detonation at cryogenic temperatures is several times shorter than that at ambient conditions. This is counterintuitive since the chemical reactivity at cryogenic temperatures is expected to be much lower than that at ambient conditions.

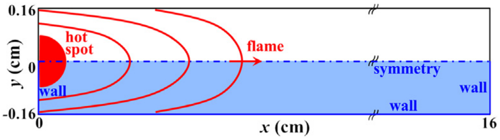

Fig. 1. Schematic of flame propagation in a narrow channel. The computational domain is in blue and the boundary conditions are indicated.

According to Valiev et al. [13], before the occurrence of DDT there are different flame acceleration stages from slow burning to Chapman-Jouguet deflagration. Besides, DDT usually happens in confined space. Therefore, better understanding of the early stage of flame propagation and acceleration in tubes/channels assumes critical importance. Though many studies (e.g., [13–16]) have been conducted for flame propagation and acceleration in tubes/channels, there is little work on the propagation of premixed H_2/air flames at cryogenic temperatures. Currently, there is still incomplete understanding of the flame behavior for cryogenic hydrogen, which has direct implications for safe utilization of hydrogen.

Based on the above-mentioned considerations, the objective of this work is to assess and interpret the effects of extremely low temperature on premixed hydrogen/air flames propagating in a closed channel. Different initial temperatures ranging from normal temperature ($T_0 = 300$ K) to cryogenic temperature ($T_0 = 100$ K) are considered. Both 1D and 2D simulations are conducted, and detailed chemistry and transport are considered. The 1D and 2D flame propagation is compared, and different stages of flame propagation are identified and discussed for different initial temperatures of $T_0 = 100$, 200 and 300 K.

2. Numerical models and methods

We consider premixed H_2/air flames propagating in a closed, narrow channel. Note that here we consider flame propagation in a closed channel, in which the pressure waves reflect on the end wall. In an open channel, the flame propagation behavior will be different. As showed in Fig. 1, the channel length and width are 16 cm and 0.32 cm, respectively. Due to symmetry, the computational domain with $L = 16$ cm and $h = 0.16$ cm is half of the whole physical region. The boundary conditions are also depicted in Fig. 1 and the wall is assumed to be adiabatic, no-slip and inert (i.e., no surface reaction).

Initially the closed channel is filled with quiescent, stoichiometric H_2/air mixture at the atmo-

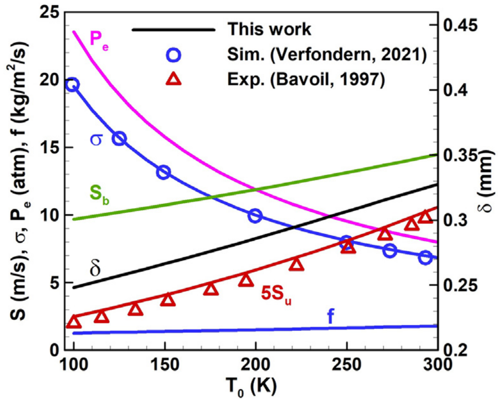

Fig. 2. Properties of steady, planar, premixed H_2/air flames at atmospheric pressure and different initial temperatures. S_u and S_b are laminar flame speed relative to the unburned and burned gas, respectively. $f = \rho_u S_u$ is the laminar burning flux, δ the flame thickness, σ the expansion ratio, and P_e the equilibrium pressure. The symbols represent laminar flame speeds (S_u) measured in experiments and the expansion ratio (σ) calculated using a real gas equation of state reported in [3,22].

spheric pressure, $P_0 = 1$ atm. The initial temperature of the fresh mixture is case-dependent, from cryogenic condition of $T_0 = 100$ K to normal condition of $T_0 = 300$ K. The temperature between them, $T_0 = 200$ K, is also considered. As shown in Fig. 1, the flame is ignited by a semicircle hot spot, whose center is at $x = y = 0$ cm. The temperature and radius of the hot spot are fixed to be 1500 K and 0.8 mm, respectively.

Besides the 2D flame propagation depicted in Fig. 1, we also consider the 1D premixed H_2/air flames propagating in a closed chamber with the same length of 16 cm. Similar to the 2D flame, the 1D flame is also initiated by a hot region at the left side and the initial and boundary conditions are same as those on the symmetry line shown in Fig. 1. Flame surface area change occurs only in 2D case which makes the combustion process in 2D case completely different from 1D case.

The transient 1D and 2D flame propagation processes are simulated using the solver A-SURF [17] and PeleC [18], respectively. In both A-SURF and PeleC, the fully compressible governing equations for multi-component reactive flows are solved using the finite volume method. The details on the governing equations and numerical methods can be found in the documents in [17,18]. To accurately and efficiently resolve the propagation of flame and pressure wave, adaptive mesh refinement algorithm is used in both solvers. The reaction zone is always fully covered by the finest grid size of 3.125 μm, which ensures that grid independence is achieved. Both A-SURF and PeleC have been used in previous studies (e.g., [17,19,20]) on flame propagation in a closed chamber.

The detailed kinetic model for hydrogen developed by Konnov [21] is used in all simulations. The mechanism at cryogenic temperature has been validated before simulations and the details are provided in the Supplemental Document. Fig. 2 shows that for $100 \leq T_0 \leq 300$ K, the laminar flame speed predicted by this kinetic model agrees well with the experiment data of Bavoil [3,22]. The multi-component model is used to calculate the mass diffusion coefficients for all species. The evaluation of kinetic model, thermal and transport properties within $100 \leq T_0 \leq 300$ K is described in the Supplementary Material. The ideal gas law is used here. Fig. 2 shows that the present expansion ratio, σ (density ratio between unburned and burned gasses, i.e., $\sigma = \rho_u/\rho_b$), agrees very well with that calculated using a real gas equation of state [3].

3. Results and discussion

3.1. Properties of steady, planar, premixed flame

We first investigate the properties of 1D steady, planar, premixed H_2/air flames for $100 \leq T_0 \leq 300$ K. Specifically, the laminar flame speed relative to unburned and burned gasses, S_u and S_b, the laminar burning flux, $f = \rho_u S_u$, and the flame thickness defined based on maximum temperature gradient, δ, are calculated using Cantera [23]. The results are shown in Fig. 2, in which the expansion ratio, σ, and the equilibrium pressure of constant volume combustion, P_e, are also plotted. As expected, the expansion ratio and equilibrium pressure both increases greatly as the temperature decreases. The laminar flame speed relative to unburned gas decreases significantly from $S_u = 2.1$ m/s at $T_u = 300$ K to $S_u = 0.5$ cm/s at $T_u = 100$ K. Compared to S_u, the change in S_b is much more moderate since $S_b = \sigma S_u$. Similarly, the laminar burning flux, f, is shown to be insensitive to the initial temperature. Surprisingly, the flame is shown to be thinner at lower temperature. At lower initial temperature, the flame thickness becomes smaller and the expansion ratio becomes larger, and thereby the flame becomes more unstable due to the probable Rayleigh-Taylor instability (RTI) and Darrieus-Landau instability (DLI, or hydrodynamic instability) [24]. This means that the flame front is more unstable at cryogenic temperature compared to the normal temperature.

3.2. One-dimensional flame propagation

The 1D flame propagation is mainly controlled by the laminar flame speed since there is no flame surface area change. Note that in a closed chamber, the unburned gas is compressed during flame

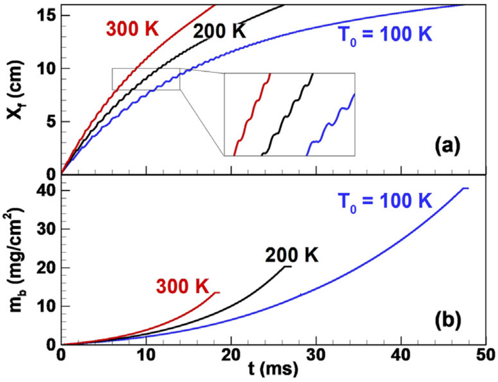

Fig. 3. Temporal evolution of (a) flame position, X_f, and (b) mass of burned gas, m_b, for different initial temperatures.

propagation and thereby its temperature and pressure increase continuously [17,19]. Fig. 3(a) compares the evolution of flame position (defined as the position with maximum heat release rate) for different initial temperatures. It is seen that the flame propagates slower at lower initial temperature. At the beginning (end) of the whole process, the absolute flame propagation speed, $S = dX_f /dt$, is close to S_u (S_b) since the burned (unburned) gas is nearly static. Since both S_u and S_b are smaller for lower initial temperature (see Fig. 2), the combustion duration, t_d, increases as the initial temperature decreases: t_d = 18.1, 26.3 and 47.4 ms for T_0 = 300, 200 and 100 K, respectively. Note that the insert in Fig. 3(a) shows that the flame position does not increase smoothly with time. Strong oscillation in absolute flame propagation speed is observed (not shown here), which is caused by pressure wave-induced backward and forward flow in the closed chamber [17]. Since stronger pressure wave is induced at lower T_0 with larger energy density, the non-smoothness of flame position is strongest at T_0 = 100 K as shown in the insert in Fig. 3(a).

The evolution of burned mass, m_b, is plotted in Fig. 3(b). It is seen that the time derivative of m_b, i.e., dm_b/dt, increases with time. This is because the temperature and pressure of unburned gas continuously increase with time and so does the laminar burning flux (note that for 1D flame we have $dm_b/dt = f = \rho_u S_u$). Even at the end of combustion, dm_b/dt is smaller at lower initial temperature. Therefore, the local burning rate for unit flame surface is always weaker at lower initial temperature. However, this does not mean that the combustion process for hydrogen at cryogenic temperature is slower than that at normal temperature in reality. The flame surface area also affects the burning time, which shall be investigated in the following subsection.

3.3. Two-dimensional flame propagation

Unlike 1D flame which cannot take account of flame surface area change and side wall boundary condition, 2D flame does not remain flat and the flame surface corrugates considerably due to the existence of side wall and different types of instabilities that might appear during combustion process. Shortly after ignition, the flame propagating in the narrow channel is curved and elongated due to the constraint of no-slip side wall. This phenomenon can be more significant at lower initial temperature due to larger expansion ratio. The omnipresent Darrieus-Landau instabilityalways wrinkles the flame front and it is caused by the density jump across the flame front [24]. Since the expansion ratio increases greatly as the temperature decreases to cryogenic value (see Fig. 2), DLI is expected to be very strong at extremely low initial temperature. Besides, in a closed chamber, pressure wave interacts with the density jump across the flame front and induces the Rayleigh-Taylor instability. According to Petchenko et al. [25] and Xiao et al. [26], RTI can significantly increase the flame front distortion and thereby increases the global burning rate. Since stronger pressure wave is induced at lower initial temperature with larger energy density, the influence of RTI is also expected to be very strong at extremely low initial temperature. Consequently, both the existence of side wall and the appearance of DLI and RTI can substantially increase the flame surface area and thereby accelerate flame propagation in H_2/air mixtures at cryogenic temperatures.

Fig. 4 shows the temporal evolution of flame position along the center line and the corresponding absolute propagation speed for different initial temperatures. Note that the flame front along the center line is not always the flame tip because the flame front topology varies dramatically during the combustion process (see Fig. 10 shown later). For instance, when the so-called “tulip flame” is formed, the flame is concave toward the burned gas. Nevertheless, the global flame dynamics can still be reflected, at least qualitatively, by the flame position history along the center line.

Fig. 4(a) shows that there is strong oscillation in the flame position. As mentioned before, such oscillation is caused by the back-and-forth propagation of pressure wave. When the pressure wave propagates from the right to the left, the flow pushes the flame front toward the left side and thereby the absolute flame propagation speed becomes negative (see Fig. 4b). Both Fig. 4(a) and 4(b) indicate that the oscillation is stronger at lower initial temperature. This is attributed to the stronger pressure wave induced at lower initial temperature.

Comparison between 1D and 2D results in Figs. 3(a) and 4(a) reveals that the oscillation is much stronger in 2D case. Furthermore, Fig. 4(a) shows that the combustion duration, t_d, decreases

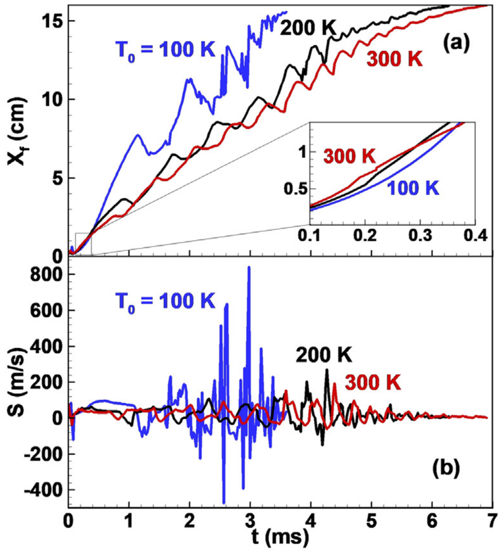

Fig. 4. Temporal evolution of (a) flame position X_f along the central line at $y = 0$ cm and (b) corresponding absolute flame propagation speed $S = dX_f/dt$ for different initial temperatures.

as the initial temperature decreases: t_d = 7.0, 6.3 and 3.6 ms respectively for T_0 = 300, 200 and 100 K, while the opposite occurs for 1D case. The combustion duration ratio between 1D and 2D cases increases significantly with the decrease of the initial temperature: $t_{d,\mathrm{1D}}/t_{d,\mathrm{2D}}$ = 2.6, 4.2 and 13.2 respectively for T_0 = 300, 200 and 100 K. Therefore, the increase of flame surface caused by the no-slip side wall and combined effects of DLI and RTI can drastically accelerate the burning of hydrogen at cryogenic temperatures, which brings great concerns for hydrogen safety. These results also help to explain the counterintuitive observation by Kuznetsov et al. [12] that the run-up-distance to detonation at cryogenic temperatures is much shorter than that at normal temperatures.

Note that the insert in Fig. 4(a) shows that similar to 1D flame, the 2D flame initially propagates faster at higher initial temperature. This is because at the beginning the influence of side walls is small and the flame propagation is mainly controlled by the laminar flame speed relative to burned gas, which increases with the initial temperature (see Fig. 2). After the flame touching the side wall, the 2D flame propagates faster at lower initial temperature.

To quantify the global combustion process, we plot the evolution of the burned mass for different initial temperatures in Fig. 5. It is seen that at the beginning with $t < 0.24$ ms, faster burning occurs at higher initial temperature while the opposite holds for $t > 0.4$ ms. This is consistent with the results on flame position shown in Fig. 4(a).

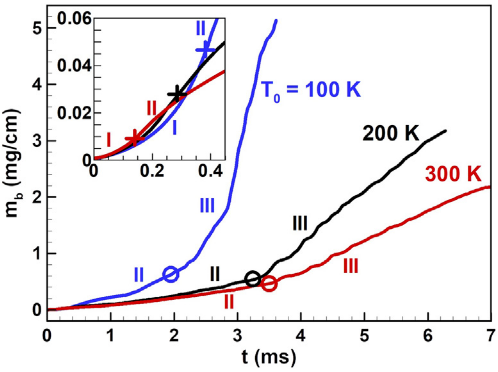

Fig. 5. Change of the burned mass with time. The symbol + separates stages I and II, and symbol ○ separates stages II and III.

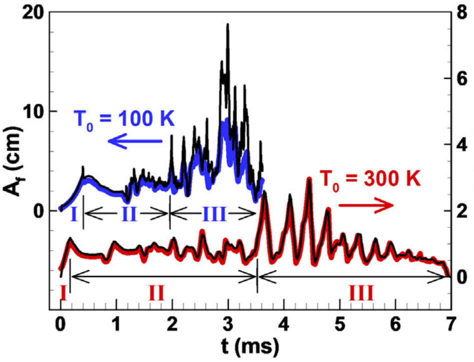

Fig. 6. Change of total flame surface area with time for T_0 = 100 and 300 K. Thin black lines represent A_f calculated based on Eq. (1) and thick color lines denote A_f based on the isosurface of $T = 1000$ K. Three stages I, II and III are marked. (For interpretation of the references to color in this figure legend, the reader is referred to the web version of this article.)

The total flame surface area, A_f (in fact it is the flame front length for 2D case and has unit of centimeter) can be determined from m_b according to:

$$A_f = (dm_b/dt)/(\rho_u S_u) \tag{1}$$

Note that ρ_u and S_u both change since the unburned gas is continuously compressed. Besides, Eq. (1) holds under the assumption that the local flame speed is not affected by flame stretch and thus the burning rate is primarily controlled by the flame surface area. The flame surface area can also be determined based on the isosurface of temperature, e.g., T = 1000 K. Fig. 6 plots the temporal evolution of A_f. For T_0 = 300 K, A_f determined from both methods is shown to be almost identical. For T_0 = 100 K, though obvious difference is observed for A_f determined from these two methods, the same oscillation in A_f is obtained. The difference might be attributed to the very large local

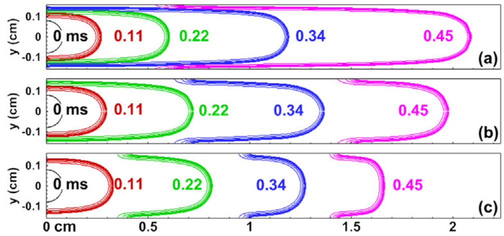

Fig. 7. Sequences of temperature contour lines from 1200 K to 1800 K for different initial temperatures: (a) $T_0 = 100$ K, (b) $T_0 = 200$ K, and (c) $T_0 = 300$ K. See also the animation in the Supplementary Material.

flame curvature/stretch (see Fig. 10) which affects the local flame speed. Fig. 6 shows that the change in A_f at cryogenic temperature of $T_0 = 100$ K is much larger than that at normal temperature of $T_0 = 300$ K.

Based on the time derivative of burned mass, dm_b/dt, or the change in total flame surface area, A_f, the whole combustion process can be divided into three stages (as marked in Figs. 5 and 6): (I) initial acceleration stage, during which the flame propagates outwardly and thereby A_f increases rapidly; (II) steady burning stage, during which A_f does not change significantly; and (III) rapid acceleration stage, during which the intensive flame-pressure wave interaction greatly increases A_f.

Stage I ends when the flame arrives at the side wall. During stage I and at the beginning of stage II, the pressure rise is negligible and thereby the flame front is not affected by pressure waves. Fig. 7 presents the flame front propagation during stage I and the beginning of stage II. The animation of the entire flame propagation processes for $T_0 = 100$, 200 and 300 K is presented in the Supplementary Material.

Fig. 7 shows that at $t = 0.11$ ms, the flame expands toward the side walls and A_f is the largest for the highest initial temperature of $T_0 = 300$ K. This is reasonable since the laminar flame speeds relative to unburned and burned gasses both increases with the initial temperature. At $t = 0.22$ ms, the flame with $T_0 = 300$ K already reaches the side wall and its surface area abruptly decreases, whereas the flame fronts for $T_0 = 200$ and 100 K have not reached the side wall yet. Therefore, the duration of stage I is longest for the lowest initial temperature (see the insert in Fig. 5). This observation is consistent with the theoretical analysis by Valiev et al. [15], who found that the time taken for the flame to reach the side wall is

$$t_w = (h/S_u)[\ln \sigma/(\sigma - 1)] \tag{2}$$

Although the term $\ln\sigma/(\sigma-1)$ in Eq. (2) increases with the initial temperature (due to the reduction in expansion ratio σ with T_0), the reduction in t_w (due to the increase in S_u with T_0) dominates over the influence caused by expansion ratio. Consequently, t_w decreases with the initial temperature.

After the initial acceleration stage, the flame reaches the side wall and propagates toward the right side. As shown in Figs. 6 and 7, the flame surface area quickly decreases at the beginning of stage II and remains nearly constant. Fig. 7 shows that at $t = 0.45$ ms which is within stage II (see Fig. 5), A_f for $T_0 = 100$ K is much larger than that for $T_0 = 200$ and 300 K. At primarily determined by the expansion ratio according to the following expression in [15]:

$$A_f = 2h\sigma^2 \ln \sigma/(\sigma - 1) \tag{3}$$

When the initial temperature is reduced from $T_0 = 300$ K to $T_0 = 100$ K, the expansion ratio increases from $\sigma = 6.8$ to $\sigma = 19.5$, resulting in $A_{f,100\mathrm{K}} = 4A_f$,300 K according to Eq. (3). This agrees quantitatively with the results shown in Figs. 6 and 7. Therefore, reducing the initial temperature can remarkably increase the flame surface area and thereby accelerate the burning process during stage II. Note that Darrieus-Landau instability becomes strong and dominant only when a nearly planar flame can be sustained in a sufficiently uniform flow. Due to the existence of no-slip side wall, the flame could wrinkle without any perturbation and instability development. Though the flame front is curved in Fig. 7, the no-slip side wall and consequent velocity shear near the wall are important for the flame wrinkling.

During the steady burning stage II, the pressure inside the closed chamber starts to increase substantially. Consequently, the flame front interacts with the pressure waves reflected from the left and right walls. This process is shown in Fig. 8, in which the isolines for heat release rate (HHR) represent the flame front position and finite flame thickness. Note that only the lower half of the physical domain is presented. Fig. 8 depicts three collisions between the flame front and pressure wave for $T_0 = 200$ K. At $t = 866$ μs, the pressure wave and the flame front propagate toward each other. Then the first collision between them takes place at around $t = 878$ μs, which results in a reflected pressure wave propagating to the right wall and a transmitted pressure wave propagating to the left wall. Since the transmitted pressure wave is close to the left wall, it quickly reflects on the left wall and catches up with the flame front (see the frame at $t = 943$ μs in Fig. 8). The second collision between flame and pressure wave occurs at around $t = 949$ μs, which further results in a reflected pressure wave propagating leftwards and a transmitted pressure wave propagating rightwards. The reflected pressure wave reflects on the left wall at around $t = 1000$ μs and then it collides with the flame front at around $t = 1023$ μs. Fig. 8 shows that the flame surface area changes non-monotonically and the integrity and smoothness of the flame front are generally maintained during these collisions.

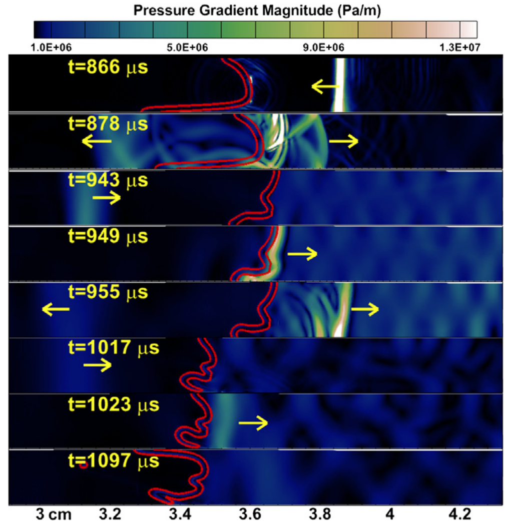

Fig. 8. Temporal evolution of flame-pressure wave interaction for $T_0 = 200$ K. Red lines represent the isolines of HRR = 10^{10} W/m^3, arrows denote the directions of the pressure wave propagation, and the contour color reflects the magnitude of the pressure gradient. See also the animation in the Supplementary Material. (For interpretation of the references to color in this figure legend, the reader is referred to the web version of this article.)

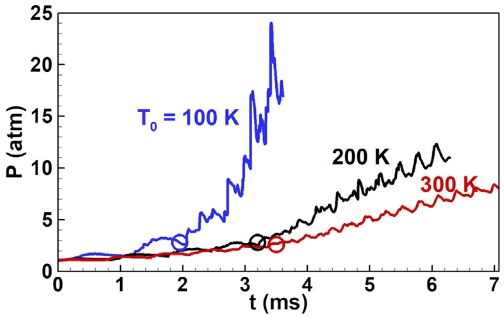

Fig. 9. Pressure histories recorded on left wall for different initial temperatures. The symbol ○ separates stages II and III.

Similar interaction between flame and pressure wave is also observed for $T_0 = 100$ and 300 K. For all T_0, strong flame front wrinkling can be observed during the multiple flame-pressure wave interactions. It is found that the flame front wrinkling is stronger at lower T_0. This is because stronger pressure wave appears at lower T_0 as mentioned before. Besides, once the flame front is wrinkled, the disturbance grows faster for larger expansion ratio at lower T_0 [26].

Fig. 9 plots the recorded pressure histories near the left wall for different T_0. Within stage II the pressure rise is relatively low. As the pressure wave reflects on the wall the pressure recorded near the wall suddenly increases and thereby many spikes can be observed in Fig. 9. After the flame transits into stage III, the pressure is shown to rise much faster with stronger oscillation than that in stage II. This indicates that very intensive burning occurs during stage III.

Fig. 10 shows the evolution of the flame front within stage III. As expected, the flame front is violently folded and the surface area increases dramatically (see also Fig. 6). The flame front is shown to be broken into multiple fragments at $t = 2.59$ ms in Fig. 10(a), $t = 3.67$ ms in Fig. 10(b), and $t = 3.67$ and 4.48 ms in Fig. 10(c). Besides, the flame front is pushed back toward the left side ($t = 2.7$ ms in Fig. 10a and $t = 3.4$ ms in Fig. 10b). These are caused by the combined effects of DLI and RTI related to strong flame-pressure wave interaction.

Moreover, Fig. 10 shows that the flame front wrinkling is much more distinct at lower initial temperature T_0. This can be explained by the combined effects of DLI and RTI mentioned before. At lower T_0, the equilibrium pressure is higher (see Fig. 2) and so is the pressure in the closed chamber (see Fig. 9). Consequently, the flame becomes thinner at lower T_0. Besides, the density jump (i.e., the expansion ratio) is larger for lower T_0. These two factors both enhance the instabilities at low T_0. Note that in stage III DLI may also have contribution to flame surface area increase since wrinkles with different wavelengths are observed in Fig. 10. This is reasonable since in stage III the pressure is greatly elevated from 1 atm to about 15 atm or more and channel width is at least an order of magnitude larger than the flame thickness, especially for the cryogenic temperature case.

RTI also depends on the expansion ratio and its nondimensional growth rate is [26]

$$\omega_{RT} = \omega^*_{RT}/kS_u = \sqrt{[1-2/(\sigma+1)]a/S_u^2 k} \qquad (4)$$

where k is the wave number and a is the acceleration factor. However, in this formula only RTI is considered. Therefore, to assess the combined effects of DLI and RTI, the nondimensional growth rate ω is [27,28]

$$\omega = \frac{\sigma}{\sigma+1}\left(\sqrt{\sigma - \frac{1}{\sigma} + 1 + \frac{\sigma^2-1}{\sigma^2}\frac{a}{S_u^2 k}} - 1\right) \qquad (5)$$

where the growth rate is scaled by kS_u. The acceleration factor positively correlates with the amplitude of pressure oscillation, which is larger at lower T_0 (see Fig. 9). Therefore, for lower T_0 we have larger a and σ and smaller S_u, and thereby larger growth rates ω_{RT} and ω for the given wave number k according to Eqs. (4) and (5). Since the channel width is the same in all simulations, the characteristics wave number k is approximately equal for these three cases. This indicates that stronger instabilities occur at lower T_0. In this context, both DLI and RTI contribute to the significant increase in the flame surface for hydrogen at cryogenic temperature. Noted that the diffusional-thermal instability

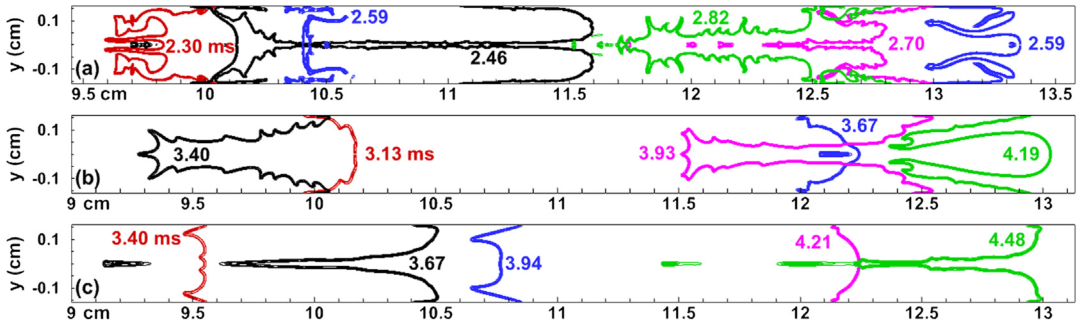

Fig. 10. Temporal evolution of the flame front for (a) T_0 = 100 K, (b) T_0 = 200 K and (c) T_0 = 300 K. See also the animation in the Supplementary Material.

is not considered here since it has weak influence on a stoichiometric H_2/air mixture whose Lewis number is close to unity [24,26].

It is noted that the flame surface area increase in different stages is more pronounced for larger expansion ratio. However, the detailed mechanisms are different. In stage I and stage II, the flame front is curved by the side wall, while in stage III the flame wrinkles are caused by the instabilities. Though the flame surface area increases with expansion ratio in stage I and stage II, it is the result of side wall rather than instabilities which can also be enhanced with expansion ratio.

4. Conclusions

The propagation and acceleration of premixed H_2/air flames in a closed, narrow channel are investigated through one- and two-dimensional simulations considering detailed chemistry and transport. Different initial temperatures ranging from normal temperature (T_0 = 300 K) to cryogenic temperature (T_0 = 100 K) are considered. The effects of extremely low initial temperature on flame propagation and acceleration are assessed and interpreted.

It is found that when the initial temperature decreases from T_0 = 300 K to T_0 = 100 K, the expansion ratio and equilibrium pressure both increase substantially while the laminar flame speeds relative to unburned and burned gasses decrease moderately. Since the 1D flame propagation without flame surface area change is determined by laminar flame speed, the 1D combustion duration increases as the initial temperature decreases. However, the opposite trend is found for 2D flames. This is mainly due to the effect of side wall and flame instability occurring in 2D flames. Based on the change in total flame surface area, the whole combustion process in a closed channel can be divided into three stages: (I) initial acceleration stage, (II) steady burning stage, and (III) rapid acceleration stage. It is found that stage I is the longest for the lowest initial temperature since it is mainly determined by the laminar flame speed. For the steady burning stage, the flame surface area is mainly determined by the expansion ratio and thus increases considerably as the initial temperature decreases. This indicates that reducing the initial temperature can remarkably increase the flame surface area and thereby accelerate the burning process during stage II. Multiple flame-pressure wave interactions are observed and they can remarkably change the shape of flame front. During the rapid acceleration stage, the flame surface area increases dramatically due to the flame instability related to flame-pressure wave interaction. Both Darrieus-Landau instability and Rayleigh-Taylor instability are found to be stronger at lower initial temperature, and thereby can significantly increase the global burning rate of hydrogen at cryogenic temperatures.

This study demonstrates that flame propagation and acceleration in a closed channel become very fast at cryogenic temperature. The present results help to partly explain the counterintuitive observation in [12,29] that the run-up-distance to detonation at cryogenic temperatures is much shorter than that at normal temperatures. In future works, the DDT processes at different initial temperatures shall be studied. Besides, this study considers a thin channel with the width of 0.32 cm and the pressure is fixed to be 1 atm. It would be interesting to assess the effects of channel width and pressure [30] on the hydrogen/air flame propagation at cryogenic temperatures.

Declaration of Competing Interest

The authors declare that they have no known competing financial interests or personal relationships that could have appeared to influence the work reported in the paper

Acknowledgements

This work was funded by National Natural Science Foundation of China (Nos. 52176096 and 52006001). We thank Dr. Yiqing Wang at Peking University, China and Dr. Mike Kuznetsov at Karlsruhe Institute of Technology, Germany for helpful discussion. The suggestions from anonymous reviewers are also thanked.

Supplementary materials

Supplementary material associated with this article can be found, in the online version, at doi:10.1016/j.proci.2022.08.091.

References

[1] Z. Abdin, A. Zafaranloo, A. Rafiee, W. Mérida, W. Lipiński, K.R. Khalilpour, Hydrogen as an energy vector, Renew. Sust. Energ. Rev 120 (2020) 109620.

[2] A.L. Sánchez, F.A. Williams, Recent advances in understanding of flammability characteristics of hydrogen, Prog. Energy Combust. Sci. 41 (2014) 1–55.

[3] K. Verfondern, D. Cirrone, V. Molkov, D. Makarov, S. Coldrick, Z. Ren, J. Wen, C. Proust, A. Friedrich, T. Jordan, M. Kuznetsov, Handbook of hydrogen safety: chapter on LH2 safety, https://hysafe.info/wp-content/uploads/sites/3/2021/06/2021-01-PRESLHY_ChapterLH2-v4.pdf.

[4] E. Abohamzeh, F. Salehi, M. Sheikholeslami, R. Abbassi, F. Khan, Review of hydrogen safety during storage, transmission, and applications processes, J. Loss Prev. Process. Ind. 72 (2021) 104569.

[5] F. Yang, T. Wang, X. Deng, J. Dang, Z. Huang, S. Hu, Y. Li, M. Ouyang, Review on hydrogen safety issues: incident statistics, hydrogen diffusion, and detonation process, Int. J. Hydrogen Energy 46 (2021) 31467–31488.

[6] A. Friedrich, W. Breitung, G. Stern, A. Veser, M. Kuznetsov, G. Fast, B. Oechsler, N. Kotchourko, T. Jordan, J.R. Travis, J. Xiao, M. Schwall, M. Rottenecker, Ignition and heat radiation of cryogenic hydrogen jets, Int. J. Hydrogen Energy 37 (2012) 17589–17598.

[7] P.P. Panda, E.S. Hecht, Ignition and flame characteristics of cryogenic hydrogen releases, Int. J. Hydrogen Energy 42 (2017) 775–785.

[8] Z. Ren, J.X. Wen, Numerical characterization of under-expanded cryogenic hydrogen gas jets, AIP Adv. 10 (2020) 095303.

[9] F.L. Dryer, M. Chaos, Z. Zhao, J.N. Stein, J.Y. Alpert, C.J. Homer, Spontaneous ignition of pressurized releases of hydrogen and natural gas into air, Combust. Sci. Technol. 179 (2007) 663–694.

[10] H.J. Lee, J.H. Park, S.D. Kim, S. Kim, I.-S. Jeung, Numerical study on the spontaneous-ignition features of high-pressure hydrogen released through a tube with burst conditions, Proc. Combust. Inst. 35 (2015) 2173–2180.

[11] E.S. Oran, Understanding explosions – From catastrophic accidents to creation of the universe, Proc. Combust. Inst. 35 (2015) 1–35.

[12] M. Kuznetsov, A. Denkevits, A. Veser, A. Friedrich, G. Necker, T. Jordan, Shock tube experiments on flame propagation regimes and critical conditions for flame acceleration and detonation transition for hydrogen-air mixtures at cryogenic temperatures, International Conference on Hydrogen Safety, 2021 online conference.

[13] D.M. Valiev, V. Bychkov, V. Akkerman, L.E. Eriksson, Different stages of flame acceleration from slow burning to Chapman-Jouguet deflagration, Phys. Rev. E Stat. Nonlin. Soft. Matter. Phys. 80 (2009) 036317.

[14] V. Bychkov, V.y. Akkerman, G. Fru, A. Petchenko, L.-E. Eriksson, Flame acceleration in the early stages of burning in tubes, Combust. Flame 150 (2007) 263–276.

[15] D.M. Valiev, V.y. Akkerman, M. Kuznetsov, L.-.E. Eriksson, C.K. Law, V. Bychkov, Influence of gas compression on flame acceleration in the early stage of burning in tubes, Combust. Flame 160 (2013) 97–111.

[16] J. Melguizo-Gavilanes, Y. Ballossier, L.M. Faria, Experimental and theoretical observations on DDT in smooth narrow channels, Proc. Combust. Inst. 38 (2021) 3497–3503.

[17] H. Yu, C. Qi, Z. Chen, Effects of flame propagation speed and chamber size on end-gas autoignition, Proc. Combust. Inst. 36 (2017) 3533–3541.

[18] M.S. Day, R.W. Grout, AMReX-combustion repository on gitHub (2021), https://github.com/AMReX-Combustion/PeleC, (Accessed April 14, 2021).

[19] H. Yu, Z. Chen, End-gas autoignition and detonation development in a closed chamber, Combust. Flame 162 (2015) 4102–4111.

[20] Y. Morii, A.K. Dubey, H. Nakamura, K. Maruta, Two-dimensional laboratory-scale DNS for knocking experiment using n-heptane at engine-like condition, Combust. Flame 223 (2021) 330–336.

[21] A.A. Konnov, Yet another kinetic mechanism for hydrogen combustion, Combust. Flame 203 (2019) 14–22.

[22] E. Bavoil, Etude expérimentale de l'influence de la diminution de la température initiale (jusqu'à 100 K) sur les déflagrations des mélanges H2-air Ph.D. thesis, University of Orleans, France, 1997.

[23] D.G. Goodwin, R.L. Speth, H.K. Moffat, B.W. Weber, Cantera: an object-oriented software toolkit for chemical kinetics, thermodynamics, and transport processes, https://www.cantera.org, (Accessed January 14, 2021).

[24] C.K. Law, Combustion Physics, Cambridge University Press, Cambridge, 2006.

[25] A. Petchenko, V. Bychkov, V.y. Akkerman, L.-E. Eriksson, Violent folding of a flame front in a flame-acoustic resonance, Phys. Rev. Lett. 97 (2006) 164501.

[26] H. Xiao, R.W. Houim, E.S. Oran, Effects of pressure waves on the stability of flames propagating in tubes, Proc. Combust. Inst. 36 (2017) 1577–1583.

[27] P. Clavin, G. Searby, Combustion Waves and Fronts in Flows: Flames, Shocks, Detonations, Ablation Fronts and Explosion of Stars, Cambridge University Press, Cambridge, 2016.

[28] V.V. Bychkov, M.A. Liberman, Dynamics and stability of premixed flames, Phys. Rep. 325 (2000) 115–237.

[29] M. Kuznetsov, A. Denkevits, A. Veser, A. Friedrich, Flame propagation regimes and critical conditions for flame acceleration and detonation transition for hydrogen-air mixtures at cryogenic temperatures, Int. J. Hydrogen Energy 47 (2022) 30743–30756.

[30] X. Shen, W. Fu, W. Liang, J.X. Wen, H. Liu, C.K. Law, Strong flame acceleration and detonation limit of hydrogen-oxygen mixture at cryogenic temperatures, Proc. Combust. Inst. 39 (2023) available online, doi:10.1016/j.proci.2022.07.005.